LBL-13606
Preprint

Lawrence Berkeley Laboratory
UNIVERSITY OF CALIFORNIA

Submitted to Radiation Research

PHYSICAL MEASUREMENTS WITH HIGH ENERGY RADIOACTIVE BEAMS

A. Chatterjee, W. Saunders, E.L. Alpen,
J. Alonso, and J. Scherer

November 1981

Donner Laboratory

Biology & Medicine Division

Prepared for the U.S. Department of Energy under Contract W-7405-ENG-48

DISCLAIMER

LBL-13606

Physical Measurements With High Energy Radioactive Beams

A. Chatterjee, W. Saunders, E. L. Alpen,
J. Alonso and J. Scherer

Lawrence Berkeley Laboratory
University of California
Berkeley, California 94720, USA

November 1981

This work was supported by the Office of Health & Environmental Research of the U.S. Department of Energy under Contract No. W-7405-ENG-48, and the National Institute of Health under Grant No. CA27024-02.

This manuscript was printed from originals provided by the authors.

High Energy Radioactive Beams

A. Chatterjee

Lawrence Berkeley Laboratory
Building 29 Mail Stop 100
University of California
Berkeley, California, 94720, USA

ABSTRACT

Chatterjee, A., W. Saunders, E. L. Alpen, J. Alonso and J. Scherer. Physical Measurements With High Energy Radioactive Beams. *Radiat. Res.*

Physical measurements have been made with high energy radioactive beams (positron emitters) produced as secondary particles from a heavy particle accelerator. Data are presented for water equivalent thickness of silicon diode, a comparison of Bragg peak ionization depth vs. stopping depth and differential stopping depths when a beam is intercepted by heterogeneous materials in the orthagonal direction. A special positron emitting beam analyzing (PEBA) system has been used to form images of the stopped radioactive beam. These measurements have direct impact on treatment planning of cancer patients with heavy particles. The impact of the radioactive beam in diagnostic procedures has been discussed.

KEY WORDS: physical meausurements, heavy particles, radioactive beam, diagnostic, cancer.

INTRODUCTION

Accelerated charged particles are now being used in the clinical trials of cancer patients at the Lawrence Berkeley Laboratory. Trials for several sites of interest are underway to evaluate the potential benefits of this particular modality of treatment (1). The rationale for using this type of radiation therapy is based on a possible therapeutic gain to be achieved as a result of an improved depth-dose distribution and enhanced biological response (2).

It is well known that heavy charged particles (protons, pions, helium and other high atomic number particles) exhibit a flat distribution in dose with depth till near the end of their range, where there is a many fold increase in ionization, called the Bragg peak. From the point of view of physics, this is a well understood phenomenon (3). Thus, if the energy of the beam can be properly controlled, so that the Bragg peak of ionization overlaps with the location of the tumor, one may reasonably expect to observe favorable results from radiotherapy with these particles. But how to ensure that the Bragg peak will be superimposed on the tumor volume? A slight error in the placement may cause severe overdose of a nearby vital organ besides underdosing the tumor. Exact calculation is, at best, difficult because of the variable stopping power of fat, tissue, bone, etc.

Several practical methods have been proposed to overcome this problem (4, 5, 6) and other efforts are still continuing. It is quite reasonable to expect that the full potential of the heavy particle therapy will never be realized until we are able to localize the Bragg peak at the appropriate depth in a patient and use the beam under optimal conditions.

At the Lawrence Berkeley Laboratory, we have proposed and are now developing a new radioactive beam diagnostic technique designed to optimize the use of therapeutic beams to treat cancer patients. Initial developments of energetic radioactive beams, and exploratory measurements with it, have been reported (6, 7). From our experience we believe that the success of the technique will depend, to a great extent, on the availability of a fairly intense flux of radioactive beam and also on a sensitive detection device.

The type of radioactive beam we have made measurements with are positron emitters, and they annihilate by decaying into two gamma rays at 180° phase difference. Typical examples of radioactive particles used are ^{11}C (20 min.), ^{15}O (2 min.) and ^{19}Ne (17 sec.). The numbers within the parenthesis are the half-lives.

These beams are obtained as secondary beams from the BEVALAC (8), a compound accelerator. For example, in order to obtain ^{19}Ne, one accelerates ^{20}Ne particles at sufficient flux. The radioactive particles are then produced as secondary particles from peripheral nuclear fragmentation reactions (9, 10). One can magnetically separate the desired secondary beam. The yields of these particles are about 1 part in 750 and can be obtained without any significant contamination from other fragments. As we have described earlier (7), these beams have ranges predictable from the energy and range of the parent beam. As a sensitive detection device we have been using a positron emitting beam analyzer (PEBA) which consists of two banks of NaI(Tℓ) crystals with twenty-four detectors in each bank. Details of PEBA have been published earlier (11). By detecting γ-rays from the positron annihilation process in coincidence mode between the various parts of crystals from two banks, it is possible to construct the image of the positron source, which is the stopping point of the radioactive beam in a target. By this method, we have been able to measure the mean range of an energetic radioactive beam with an accuracy of $\pm$ 1 mm. Availability of radioactive beams is rather a new development. Several physical measurements must be made, both in simple targets (lucite, polyethylene, etc.) as well as in animals, before one can use these beams for Bragg peak localization in patients. In this report we want to present the results of experimental measurements such as (i) comparison between the parent beam and the radioactive beam in terms of water equivalent thickness estimates, (ii) Bragg peak to mean range separation distance for a radioactive beam, and (iii) the resolution power of PEBA when a significant part of the beam goes through a denser medium such as bone. All these measurements have direct consequences in treatment planning using high radioactive beam as will be noted in the next section.

METHODS AND MATERIALS

Water equivalent thickness of silicon diode: The purpose of this measurement was to estimate the water equivalent thickness of a silicon diode.

Data were taken with both ^{20}Ne primary beam and the ^{19}Ne secondary beam. From the stopping power theory it is well known that the water equivalent thickness should be independent of the particle charge, mass or energy.

There are two main reasons for making these measurements. First, the ^{19}Ne beam is produced from the peripheral nuclear fragmentation collision between the parent beam of ^{20}Ne and a one-inch thick Beryllium target. Thus, ^{19}Ne can be produced at any depth in the Beryllium target. Also, the secondary fragment ^{19}Ne can have any velocity according to the Gaussian distribution with the most probable value being the velocity of the parent particles. Hence, the ^{19}Ne beam has more energy spread than the parent ^{20}Ne beam. For the parent beam the energy spread is only 0.1%. The question we wished to answer was; will this spread in energy have any influence on the determination of water equivalent thickness?

Secondly, silicon diodes will be used routinely in the development stage of the radioactive beam diagnostic technique. They will be used, through ionization measurements, to confirm the Bragg peak localization estimates using PEBA. For the ionization measurement with diodes, one has to make correction to estimate the actual depth of beam stopping by taking into consideration the water equivalent thickness of a silicon diode. These detectors have the advantage of cheapness, responsiveness, and adaptability for implantation in animal tissues.

In order to determine water equivalent thickness of the silicon diode, depth dose ionization curves were measured using gas filled ion-chambers, and a variable water absorber. Measurements were then made substituting the diode detector for the ion chamber. The difference in depth at which the Bragg peak occurs in the two cases yields the water equivalent thickness of the solid state detector. Both ^{20}Ne and ^{19}Ne beams were used.

A schematic view of the equipment arrangements for the ion chamber measurements is shown in Fig. 1(a). The chambers are being used routinely for dosimetry purposes. A detailed description of the dosimetry and instrumentation involved for heavy ions has been given by Lyman and Howard (12). For the ion chamber measurements, the Bragg ionization curve was measured using the variable water column varied between zero cm. and a few centimeter beyond the depth at which the Bragg peak occurs. The readings from the ion chamber I_2 was plotted after normalizing with respect to the reading from ion chamber I_1.

Experimental arrangements for data obtained with the silicon diode are represented in Fig. 1(b). A special water container was built for this purpose. The beam entrance window was made out of a very thin mylar window of negligible thickness. With the aid of cross-fired lasers, the diode was centered in the water container and as the diode was moved longitudinally, it was always along the beam line. The diode was moved by a remote control mechanism and each position was recorded through the help of a digital readout. It could be moved by a least distance of 0.01 cm. The readout was adjusted to give zero reading when the diode was just touching the mylar window.

Both ^{20}Ne and ^{19}Ne were used in the above mentioned experimental configurations. But since the ΔE and therefore the beam spread, was expected to be large, a brass collimator was used to collimate the ^{19}Ne beam. The size of the collimator was 1 cm. in diameter. This did reduce the spread in energy of the ^{19}Ne beam (at the expense of reduced flux), but still it was not as mono-energetic as the ^{20}Ne beam. Also 1 cm. will be radioactive beam size for most of our diagnostic investigations, and hence physical measurements with this particular beam and beam-size are important. Results of this comparative measurement are given in the next section.

<u>Bragg peak depth vs. stopping depth</u>: It is well known that there is a difference in the depth at which the Bragg peak occurs and the particle range. Since the PEBA detector measures the range of a radioactive beam and the therapists are interested in localizing the Bragg ionization peak on a tumor volume, it is necessary to know the difference. If the difference is large, one may have to make appropriate corrections. Such corrections are especially important if there is a radiosensitive organ adjacent to the tumor volume.

In order to design this experiment it was necessary to consider range straggling due to statistical fluctuation of energy loss. It is well known that if the path length is large compared to the mean free path for atomic collisions, the Central Limit Theorem governing mean values in a large number of sample applies. Bohr (13) argues that the straggling should be Gaussian in such a situation. The probability density of having range around R is then given by

$$(2\Pi\ \Delta\overline{R}^2)^{-1/2} \exp\left[-(R-\overline{R})^2 / 2\ \Delta\overline{R}^2\right] \qquad (1)$$

where $\overline{R}$ is the mean range and $\overline{R}^2$ is its mean square dispersion. In a typical case the value of $(\Delta\overline{R}^2)^{1/2}/\overline{R}$ may vary from a few percent to tens of percent dependent on the medium and the particle velocity and quality.

Thus, it can be predicted that, in case of penetration of a medium by a high energy radioactive beam, the range straggling will be Gaussian and the mean range is also the most probable range, i.e., the distribution is symmetric about the mean range $\overline{R}$. Hence, if we can measure the depth at which half the amount of radioactivity has passed the target position and other half is stopped before the target, we have a measurement of $\overline{R}$.

In order to demonstrate the design of the experiment let us consider Fig. 2. Besides having two ion chambers, I_1 and I_2, the variable water column on the beam line, two lucite cylinders (L_1 and L_2) were also interposed between the two banks (banks A and B). Each lucite cylinder was 4 cm. long and 3 cm. in diameter. There was an air gap of about 4 cm. between the L_1 and L_2. The following procedures were followed:

i) the water column was adjusted so that equal activity was recorded by PEBA in each of the lucite cylinders. The reading of the water column was noted as ℓ_1. Thus, the total of the water column reading and the full length of the first lucite cylinder was the mean range of the ^{19}Ne beam. Of course, it is necessary to correct the lucite density difference to water equivalent density.

ii) the second lucite cylinders, L_2, was removed and the water column was adjusted to record maximum ionization in the ion chamber I_2. Again, the thickness of the water column was recorded as ℓ_2. Then a difference in reading between ℓ_1 and ℓ_2 gave a measurement of the separation distance between the depth at which Bragg peak occurs and the mean penetration depth.

Heterogeneity orthogonal to the direction of the beam: In some therapeutic situations, only a part of the beam goes through some amount of bone followed by tissue and the other part of the beam goes through tissue only. Thus, the path length is heterogeneous, not only in the direction of the beam but also in the transverse direction.

This can be further explained by considering the experimental diagram shown in Fig. 3. A collimated beam of ^{19}Ne is monitored by the ion chamber and then a part of the beam goes through a certain thickness of plaster ($CaSO_4$ plate) before entering the long lucite absorber which simulates tissue. The other part of the beam goes through styrofoam (air) material before it is stopped in the lucite absorber. Because of the additional stopping power of the plaster, there should be two stopping depths of the radioactive beam. The PEBA image of a point source as reproduced on a video display (as shown in Fig. 4), appears somewhat like a Gaussian with a full width half maximum of 1.5 cm. Hence, the images of the two beam stopping points may or may not be resolved depending upon the thickness of the $CaSO_4$ plates. The purpose of this experiment was to determine the resolving power of PEBA with respect to two stopping points of a given radioactive beam. Measurements were made with various amounts of plaster of paris and the results are discussed in the next section.

RESULTS

Various Bragg ionization curves were obtained using both ^{20}Ne and collimated ^{19}Ne beam. Measurements were made by using ion chambers as well as silicon diodes. The Bragg ionization curve for ^{20}Ne at 383 MeV/amu, as estimated with ion chambers (see Fig. 1(a)), is seen in Fig. 5. The actual data are shown in Table I. The Bragg peak occurs at 15.2 cm. For the same beam, when a silicon diode is used (see Fig. 1(b)), the peak in ionization occurs at 14.94 cm. as seen from Fig. 6 and the corresponding Table II. The Bragg ionization curves for the ^{20}Ne beam is quite sharp indicating a very little spread in energy of the primary ^{20}Ne beam. The difference between 15.2 cm. and 14.94 cm. is 0.26 cm., which is the water equivalent thickness of the silicon diode as measured with ^{20}Ne.

Similar Bragg curves were obtained with the secondary ^{19}Ne beam and the results are shown in Figs. 7 and 8. When only ion chambers are used (as in Fig. 1(a)), the Bragg peak appeared at 10.23 cm. in contrast with the silicon diode measurement (see Fig. 1(b)) when the peak was at 9.90 cm. The difference between these two readings is 0.33 cm., the water equivalent thickness of the silicon diode as measured with the ^{19}Ne beam. Thus, we find that there is a difference of 0.07 cm. between the measurements made with primary ^{20}Ne and the secondary ^{19}Ne beam. It is well known that the water equivalent thickness should be independent of the particle charge or energy. We attribute this difference to a rather large spread in beam energy of the ^{19}Ne ions compared to the BEVALAC primary particles, such as ^{20}Ne beam. From Fig. 7 or Fig. 8, we see that the width of the Bragg peak is much wider than those in Fig. 5 or Fig. 6 as the result of increased energy spread in the ^{19}Ne beam. Clearly the water equivalent thickness of the silicon diode measured with the ^{20}Ne beam is more precise, and we have taken that experimental value as the water equivalent thickness of the diode. The range of the ^{19}Ne beam as measured from the ionization curve is 10.45 cm. at the 50% point on the downward portion of the Bragg curve.

For the measurements made to determine the difference in spatial location between the Bragg peak of ionization and the particle range, the experiment using the lucite "catchers" (as theoretically described in the section on Bragg peak location vs. stopping range) was used. The results are shown in Figs. 9(a) through (d). Refer to Fig. 2 for the experimental arrangements.

For exact localization of the stopping range, the arguments presented earlier require an adjustment of the water column path in the beam such that quantitatively half of the radioactivity is formed in each of the lucite blocks. Such an adjustment of the particle residual range must be made by trial and error. The final setting at which such a division of activity was found was a water column setting of 5.72 cm. Within one nCi, the two peaks had the same activity (see Fig. 9(d)).

Since the water column setting was equal to 5.72 cm., and the first lucite catcher was equivalent to 4.72 cm. of water, (4 cm. x ρ (= 1.18)), the estimated mean stopping range was 10.44. This value compares very favorably with the value mentioned previously of 10.45 cm. The second lucite cylinder was then removed, and the water column so adjusted that maximum ionization intensity was measured in the second ion chambers, I_2. The water column setting for this measurement was found to be 5.56 cm. The difference in spatial position of the peak of Bragg ionization and the stopping range of the particles is thus determined to be 0.16 cm., (5.72 cm. - 5.56 cm.) for the ^{19}Ne beam used in our experiments. Using the Bragg ionization curve (see Fig. 7) we find that the difference is 10.45 - 10.23 cm., of 0.22 cm., slightly more than the 0.16 cm. found with the lucite cylinders.

To demonstrate the sensitivity of the lucite block method we show two PEBA images for water column settings, slightly under range in optimal setting, and another slightly over range. In Fig. 9(b) the water column setting was 5.8 cm. Two peaks of unequal activity are seen, 28 nCi for the upstream cylinder and 22 nCi for the downstream cylinder. For a water column setting of 5.7 cm., two peaks were again seen (Fig. 9(c)), with unequal intensities; but this time the downstream cylinder had 27 nCi compared to 23 nCi in the upstream one. These data are given to show the range of certainty with which the estimate of particle range can be estimated. A difference of only 0.1 cm. gave large and identifiable differences in deposited activity and made it easy, with precision, to finally choose the appropriate water column setting to a fraction of a mm.

Some qualitative results were obtained in the experiment where a part of the beam was intercepted by plaster of paris and part styrofoam. A graphic plot of these data are shown in Figs. 10(a) through (c). In order to review these results please refer to Fig. 3 of this paper.

In this experiment, several discs of 3 cm. diameter and 5 mm thick were used and one half of each disc was made out of $CaSO_4$ and the other half of styrofoam. These discs were placed in the path in the beam as shown in Fig. 3. A long lucite cylinder was placed after the discs which was used a stopper and image of the stopping points were formed through PEBA and displayed on a video output.

In Fig. 10(a) when only one such disc was used, the two point images could not be isolated by PEBA and hence only one image appeared even though there is some indication of another image formation. But when two such discs were used, we noticed two such distinct peaks (see Fig. 10(b)). Since the beam was not very uniform across, we did not see equal intensities. The activity in one peak was about 5 times more than in the other and hence they were quite separate from each other. When three discs were interposed, two peaks appeared and in this situation the two peaks were not that well separated because about two times more intense beam went through the $CaSO_4$ plate compared to the intensity on the styrofoam side. In this case there was more interference between the two stopping points. Thus, it was clear to us that besides the amount of different materials interposed, in order to see separate images, consideration has to be made in terms of relative intensities as intercepted by the two halves. In actual therapy, situations are not so simple as planned in this experiment. Obviously, more measurements have to be made with phantoms representing more complicated situations.

DISCUSSIONS

The availability of energetic radioactive beam is a rather new development. From our limited experinece with this beam, we feel that it has a great potential for being used as a diagnostic tool in treatment planning. But before procedures for use of these beams can be adopted with confidence, their physical characteristics must be understood. Measurements such as those presented in this paper are important for the optimal use of radioactive beams in clinical situations. For example, in some circumstances it will be mandatory to have a quantitative knowledge of the difference in depths between the position of the Bragg ionization peak and the range of the particles. Typically the radiotherapist concerns himself with the region of maximum ionization, while our detector methods determine the locus of the stopping particles. Peak ionization will always be found to occur at a position which is a few millimeters short of the particle range. For the beams reported upon in this study, the difference is about 2 mm., which in some clinical situations may be extremely important. With some patients radiation therapy with heavy particles could not be implemented for lack of such knowledge (14). Typical examples of such need for precise localization are irradiation of the pituitary or small intraocular tumors, or tumors abutting the spinal cord.

From the point of view of physics, one can state that as far as a localized tumor volume is concerned, one is interested in knowing the water equivalent thickness intervening between the point of entry of the beam into the patient and the tumor volume. As mentioned earlier, this thickness is independent of the charge or energy of the radioactive beam used, hence no matter what the choice of the therapeutic beam may be, one can always use ^{19}Ne for diagnostic purposes as long as the range is adequate to reach the tumor volume.

Availability of intense flux of radioactive beam is extremely important for statistically accurate results. The accelerator parameters of BEVALAC are such that lower the atomic number the higher is the flux. Hence one may think of using ^{11}C beam instead of ^{19}Ne beam. The physical decay rate of ^{11}C beams is smaller than for ^{19}Ne beams of equal fluence by a factor of about 70 because of the difference in their half-lives. Hence we need to obtain more (by at least a factor of 70) flux of ^{11}C beam than the intensity of ^{19}Ne beam. Also, using ^{11}C beam one can irradiate with many more pulses than ^{19}Ne beam without reaching the steady state condition (in a few pulses), where the rate of decay equals the rate of deposition. For this reason we plan to make several physical measurements with ^{11}C beam in addition to those presented in this work.

We have mentioned earlier that the spread (ΔE) in a radioactive beam is generally larger than that of the parent beam, and hence a collimator had to be used to reduce this spread. The position difference between the Bragg peak and depth is also independent upon ΔE and hence the collimator size. Further measurements have to be made with different radioactive beams to evaluate this difference for various collimator sizes.

Generally, the therapeutic beam will be particles which are stable isotopes and hence they are the primary beams from the BEVALAC. For these beams the width of the Bragg peak is smaller than that of the radioactive beams. Efforts should be made to have the physical characteristics of the radioactive beam adjusted such that the difference in the width of the Bragg peaks between the unstable beam particles and the stable beam particles should be nearly zero. All the measurements reported in this work will have practical applications in treatment planning with beams of heavy particles. There are a few more measurements of the types mentioned in this report that have to be made with different radioactive beams. Extension of this work in animals and human phantoms are in progress.

ACKNOWLEDGEMENTS

We express our great appreciation of many helpful suggestions received from Dr. J. Llacer during the course of the measurements and also the expert advice from Dr. J. T. Lyman is greatly acknowledged. We wish to thank Ms. Elizabeth Guy for editing and typing the manuscript. This work was partly supported by the Office of Health & Environmental Research of the U.S. Department of Energy under Contract No. W-7405-ENG-48 and from the National Institute of Health under Grant No. CA27024-02.

FIGURE LEGENDS

Fig. 1(a). A schematic representation of the main equipments used in determining the Bragg ionization curve by using a variable water column and two ion chambers I_1 and I_2. The readings on I_2 are always normalized to that in I_1. The minimum possible path length change for the beam in the water column is 0.01 cm. Details of the ion chambers are given in reference (12).

Fig. 1(b). Instead of using the ion chambers I_2, a silicon diode was used to measure the Bragg ionization curve. The diode could be moved in the water tray by remote control device and the position could be recorded. In this case also, the readings from the silicon diode was normalized to that observed in I_1.

Fig. 2. For mean range determination, two lucite cylinders (3.2 cm. diameter, 4 cm. long) are placed in the field of view of the detectors in the two opposing banks. ^{19}Ne beam is collimated to 1 cm. size and then monitored by the ion chamber I_1. By the help of the variable water column, activity in the two adjoining lucite edges can be made equal to determine the mean range (please see text). The downstream lucite cylinder can be removed and ionization can be recorded in I_2.

Fig. 3 A schematic view of the experimental arrangements made for resolution measurement when the beam is intercepted by heterogeneous materials (Plaster and Styrofoam) in the perpendicular direction of the beam. A lucite stopper is placed right behind the heterogeneous materials. If the range differential equals the resolution of PEBA, two separable images will be formed.

Fig. 4. The distribution of activity as detected by PEBA of a point source (1 μCi) placed at x = 0 (mechanically positioned). The plot shows the exactness with which PEBA detected the centroid of the distribution of activity. The FWHM is about 1 cm. Thus, two point sources simultaneously present within 1 cm. of each other may have difficulty in getting resolved by PEBA. But for a given point source (1 μCi), PEBA can detect its location within ± 1 mm. accuracy.

Fig. 5. Experimentally measured Bragg ionization curve for pure ^{20}Ne beam in water. Both the ion chambers (see Fig. 1(a)) were used. Data are shown in Table I. The Bragg peak occurs at 15.2 cm.

Fig. 6. For the same ^{20}Ne beam as in Fig. 5, Bragg ionization measurements data are plotted. The upstream ion chamber, I_1

and the silicon diode were used as shown in Fig. 1(a). The data are represented in Table II. In this case the Bragg peak falls at a depth of 14.94 cm.

Fig. 7. Bragg ionization curve measurement for the radioactive beam ^{19}Ne. It was produced by nuclear fragmentation of the ^{20}Ne beam in a 1" Beryllium block. Both the ion chambers were used (Fig. 1(a)). The width of the Bragg peak is wider. Ionization peaks at a depth of 10.23 cm.

Fig. 8. For the same ^{19}Ne beam (as in Fig. 7), ionization vs. depth measurement curve is shown when silicon diode was used instead of the downstream in chamber I_2. Peak in ionization occurs at 9.90 cm.

Fig. 9. Activity in the two lucite cylinders are shown for different thickness of water absorber adjusted by the variable water column. The activity distribution on the left-hand side is due to the beam stopping partially in the upstream lucite cylinder. Rest of the beam stops in the downstream lucite cylinder which is the right-hand side of each activity distribution curve. In (a) water absorber is too thick to register any activity in the downstream cylinder. In (b)

and (c) still the water absorber is not adjusted properly for the activities to be equal. In (d) the activities are equal within accuracy of the experiments. Please see text for full details.

Fig. 10. Activity distribution for differential stopping of the same beam when intercepted by different materials in the perpendicular direction to the beam incidence. In (a) only one disc (5 mm. thick $CaSO_4$ and 5 mm. thick styrofoam) was used and the images of the stopping points could not be separated beyond doubt. In (b) two such discs were used and the images are well separated. In (c) three such discs were intercepted producing separable images, but demonstrating some interference between the images of the stopping points.

REFERENCES

1. J. R. Castro, J. M. Quivey, J. T. Lyman, G. T. Y. Chen, L. Kanstein and R. Walton, Heavy Ion Radiotherapy. Report No. 5610, Lawrence Berkeley Laboratory, pp. 198-218 (1977).

2. E. A. Blakely, C. A. Tobias, T. C. Yang and K. A. Smith, Cell Survival Parameters for Extended Bragg peaks. *Rad. Res.* (abstract) 74, pp. 588 (1978).

3. R. R. Wilson, Radiological Use of Fast Protons. *Radiology* 47, pp. 487-491 (1946).

4. G. T. Y. Chen, R. P. Singh, J. R. Castro, J. T. Lyman and J. M. Quivey, Treatment Planning for Charged Particle Radiotherapy. *Int. J. Radiat. Oncol. Biol. Phys.* 5, pp. 1809-1819 (1979).

5. G. W. Bennett, J. O. Archambeau, B. E. Archambeau, J. E. Meltz and C. L. Wingate, Visualization and Transport of Positron Emission for Proton Activation *in vivo*. *Science* 200, pp. 1151-1153 (1978).

6. Aloke Chatterjee, Edward L. Alpen, Cornelius A. Tobias, Jorge Llacer and J. Alonso, High Energy Beams of Radioactive Nuclei and Their Biomedical Applications. *Int. J. Radiat. Oncol. Biol. Phys.* 7, pp. 503-507 (1981).

7. J. R. Alonso, A. Chatterjee and C. A. Tobias, High Purity Radioactive Beams at the BEVALAC. *IEEE Trans. Nucl. Sci.* NS-26(1), pp. 3003-3005 (1979).

8. A. Ghiorso, H. Grunder, W. Hartsough, G. Lambertson, E. F. Lofgren, E. F. Lou, R. M. Mair, R. Mobley, R. Morgado, W. Salsig and F. Selph, The BEVALAC -- An Economical Facility for Very High Energetic Heavy Particle Research. *IEEE Trans. Nucl. Sci.* NS-20(3), pp. 155-158 (1973).

9. H. H. Heckman, D. E. Greiner, P. J. Lindstrom and F. S. Beiser, Fragmentation of Nitrogen-14 Nuclei at 2.1 GeV per Nucleon. *Science* 174, pp. 1130-1132 (1971).

10. D. E. Greiner, P. J. Lindstrom, H. H. Heckman, B. Cork and F. S. Beiser, Momentum Distributions of Isotopes Produced by Fragmentation of Relativistic C-12 and O-16 Projectiles. *Phys. Rev. Lett.* 35, pp. 152-154 (1975).

11. J. Llacer, A. Chatterjee, B. Jackson, J. Lin and V. Zunzunegi, An Imaging Instrument for Positron Emitting Heavy-Ion Beam Injection. *IEEE Trans. Nucl. Sci.* NS-26(1), pp. 634-647 (1979).

12. John T. Lyman and Jerry Howard, Dosimetry and Instrumentation for Helium and Heavy Ions. *Int. J. Rad. Oncol. Biol. Phys.* 3, pp. 81-85 (1977).

13. N. Bohr, Charged Particle Penetration Through Matter. kgl. Danske Videnskab. Selskab. Mat.-Fys. Medd. 18, No. 8 (1948).

14. Joseph R. Castro and Jeanne M. Quivey, Clinical Experience and Expectations with Helium and Heavy Ion Irradiation. *Int. J. Rad. Oncol. Biol. Phys.* 3, pp. 127-131 (1977).

TABLE I

Depth (cm.)	Relative Ionization
7.200	0.936
8.400	0.947
9.000	0.971
9.600	0.978
10.200	0.918
10.800	0.935
11.400	1.003
12.000	1.098
12.600	1.138
13.200	1.208
13.800	1.339
14.000	1.340
14.200	1.463
14.400	1.718
14.600	1.799
14.800	1.915
15.000	2.417
15.200	4.380
15.400	0.519
15.600	0.452
15.800	0.453
16.000	0.428
16.200	0.408
16.400	0.342
16.600	0.325
16.800	0.302

TABLE II

Depth (cm.)	Relative Ionization
12.000	1.035
12.600	1.097
13.200	1.207
13.800	1.347
14.400	1.673
14.600	1.892
14.800	2.402
14.900	3.067
14.920	3.103
14.940	3.161
14.960	3.083
14.980	2.998
15.000	2.679
15.020	2.271
15.040	2.271
15.060	1.721
15.080	1.516
15.100	1.193
15.120	0.864
15.140	0.704
15.160	0.485
15.180	0.413
15.200	0.340
15.220	0.344
15.240	0.331
15.260	0.332
15.280	0.321
15.300	0.317

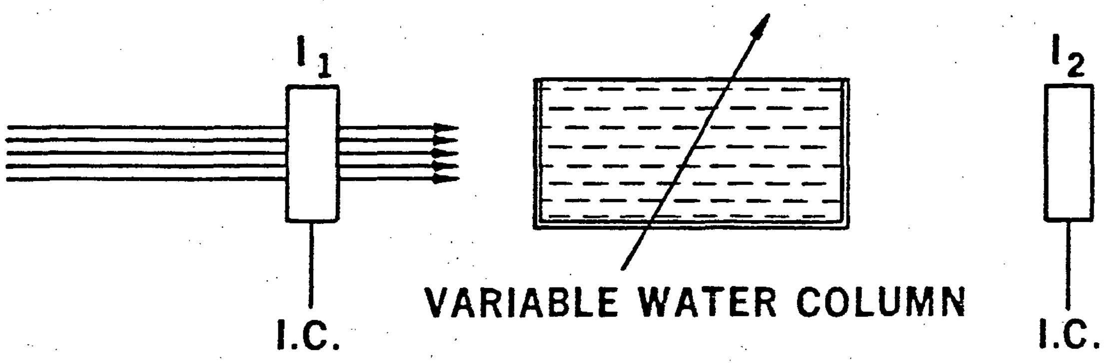

1 (a)

XBL 819-7000

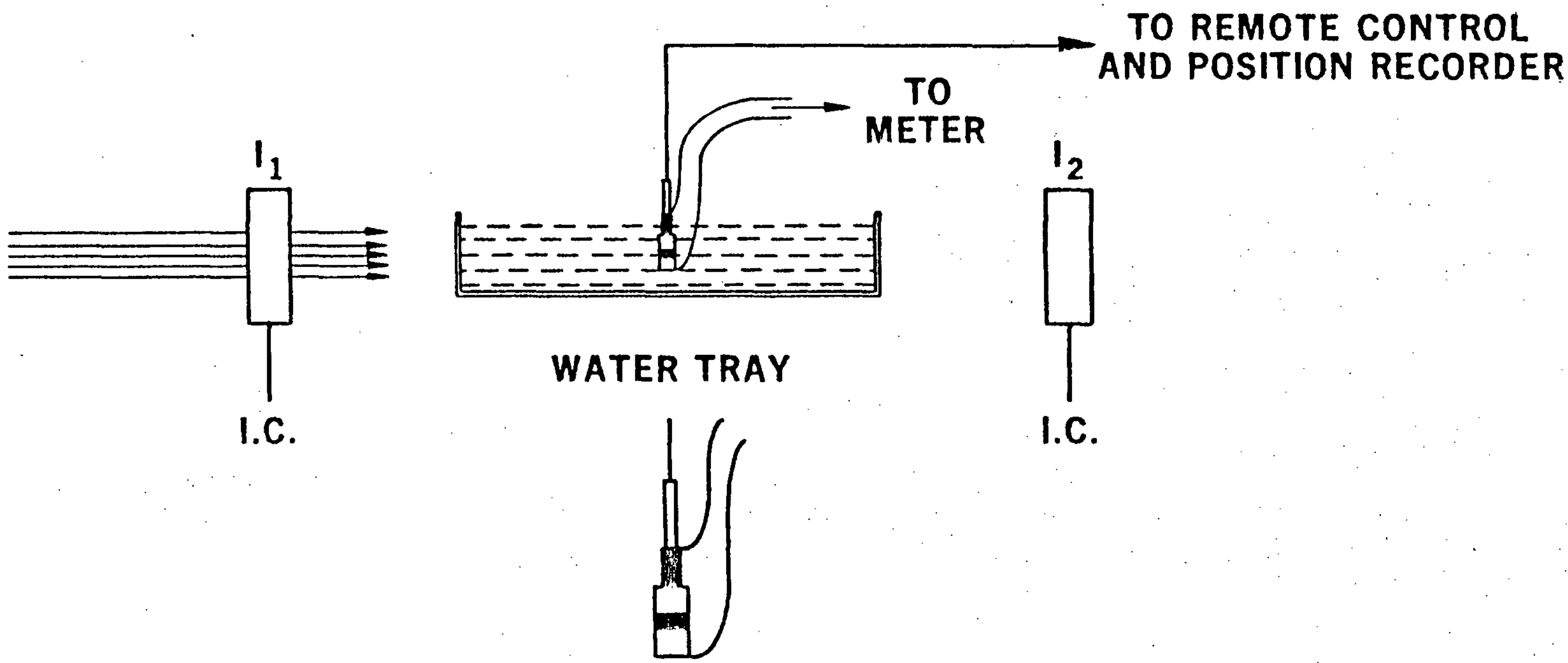

XBL 819-4999

1 (b)

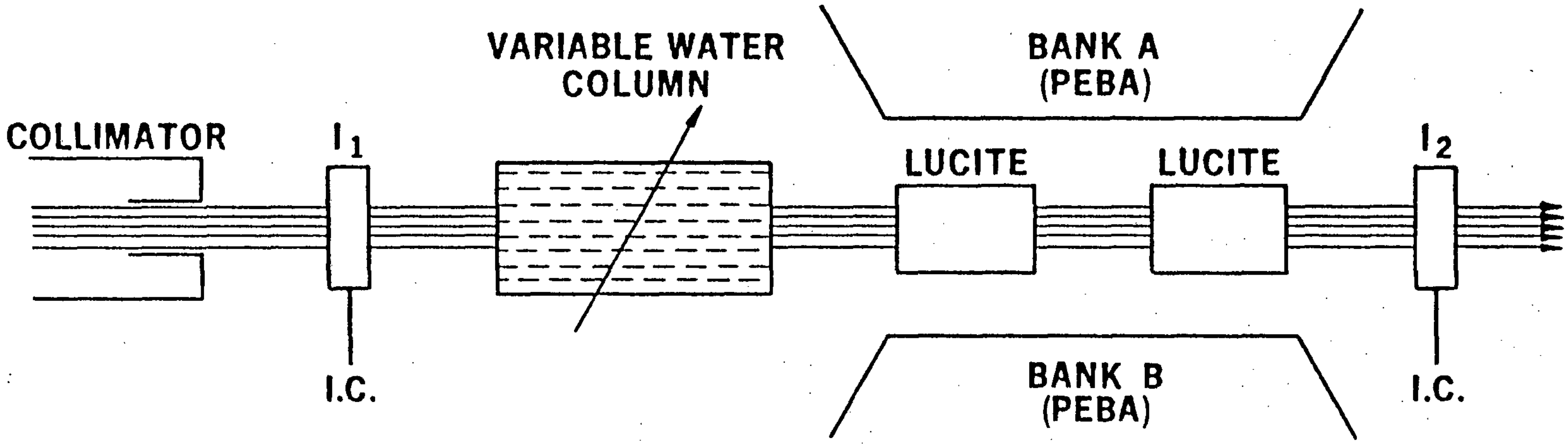
VARIABLE WATER COLUMN
BANK A (PEBA)
COLLIMATOR
I_1
LUCITE
LUCITE
I_2
I.C.
BANK B (PEBA)
I.C.

XBL 819-4998

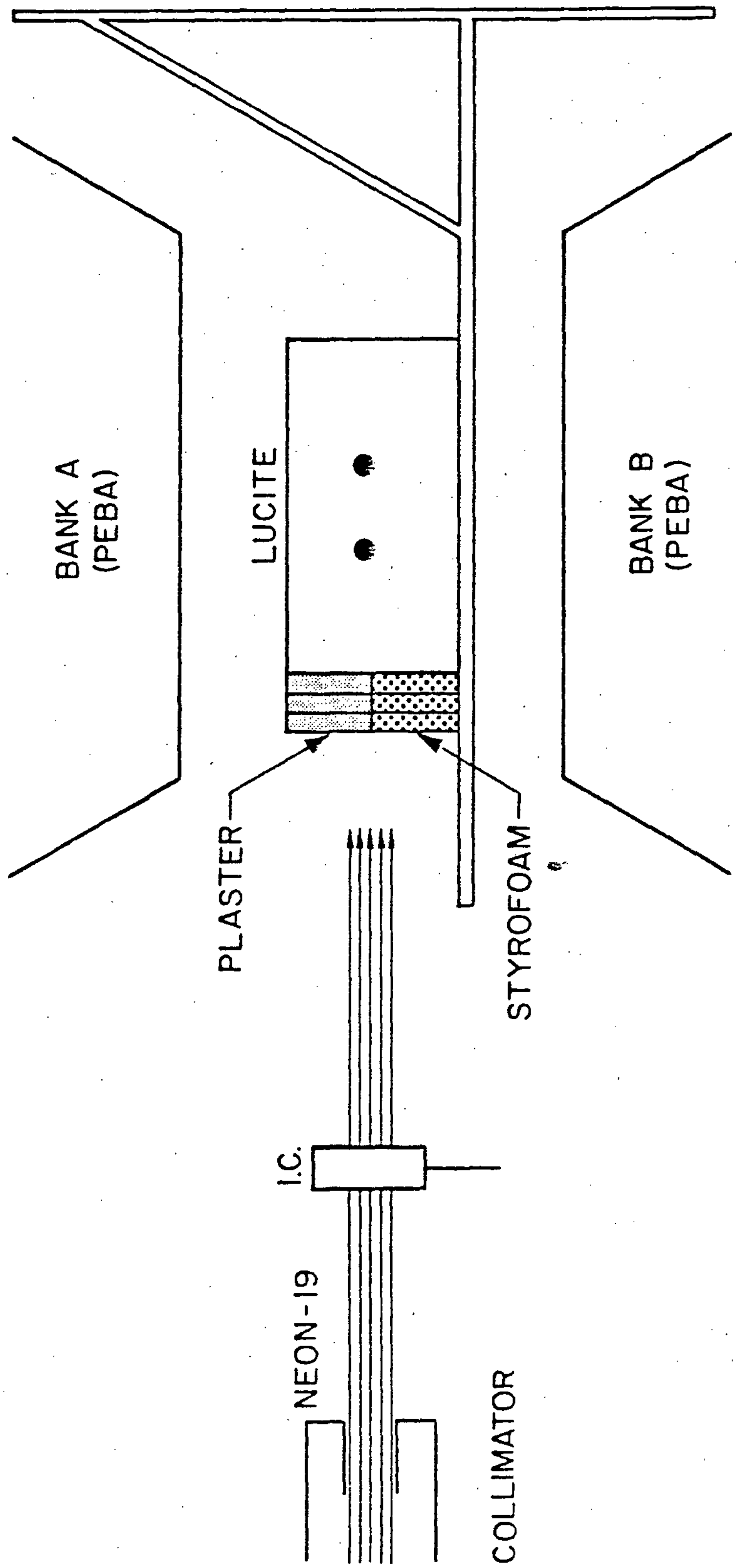
BANK A
(PEBA)
LUCITE
BANK B
(PEBA)
PLASTER
STYROFOAM
I.C.
NEON-19
COLLIMATOR

XBL 815-9855

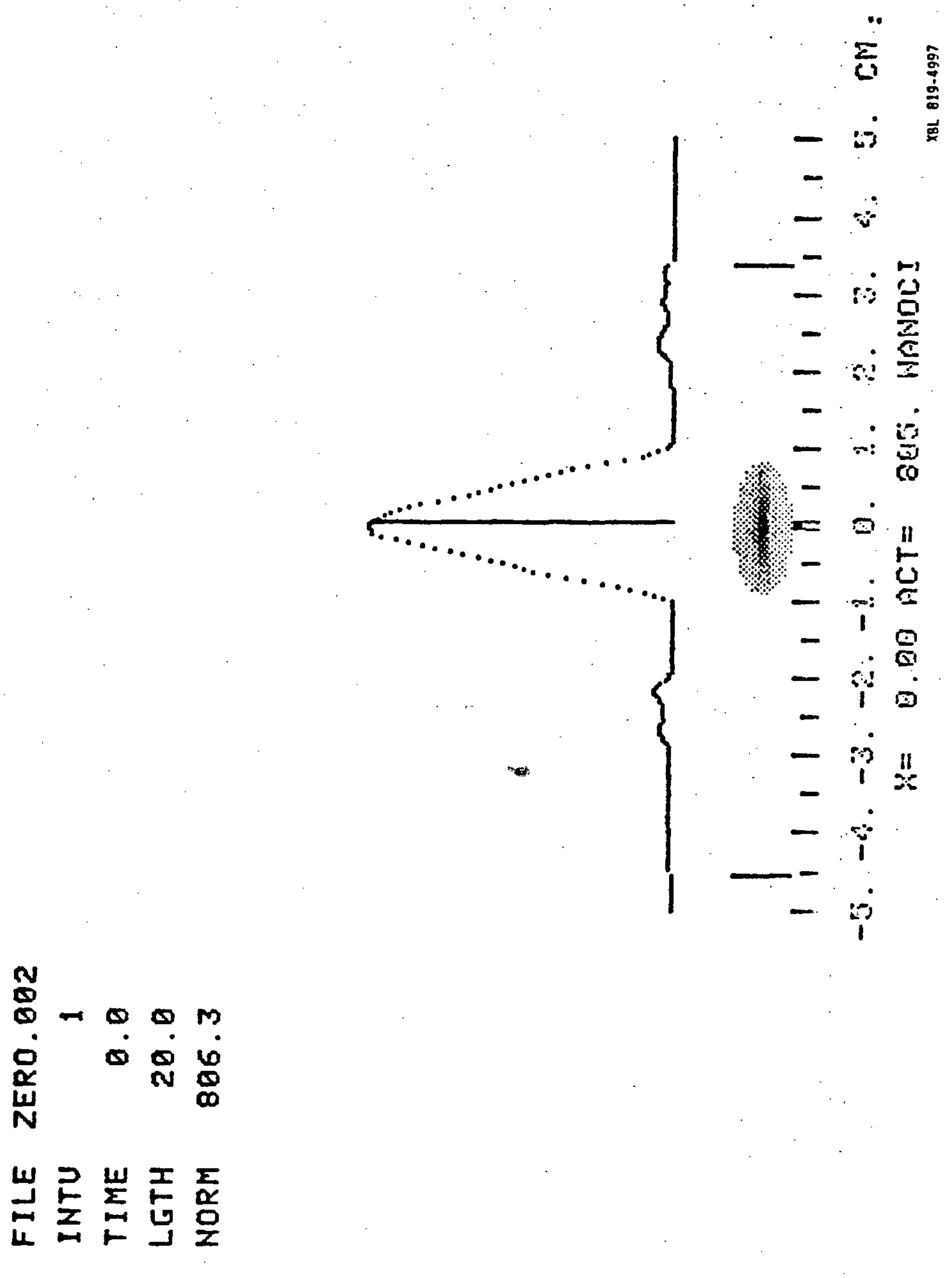
FILE ZERO.002
INTU 1
TIME 0.0
LGTH 20.0
NORM 806.3
-5. -4. -3. -2. -1. 0. 1. 2. 3. 4. 5. CM
X= 0.00 ACT= 805. WANOCI
XBL 819-4997

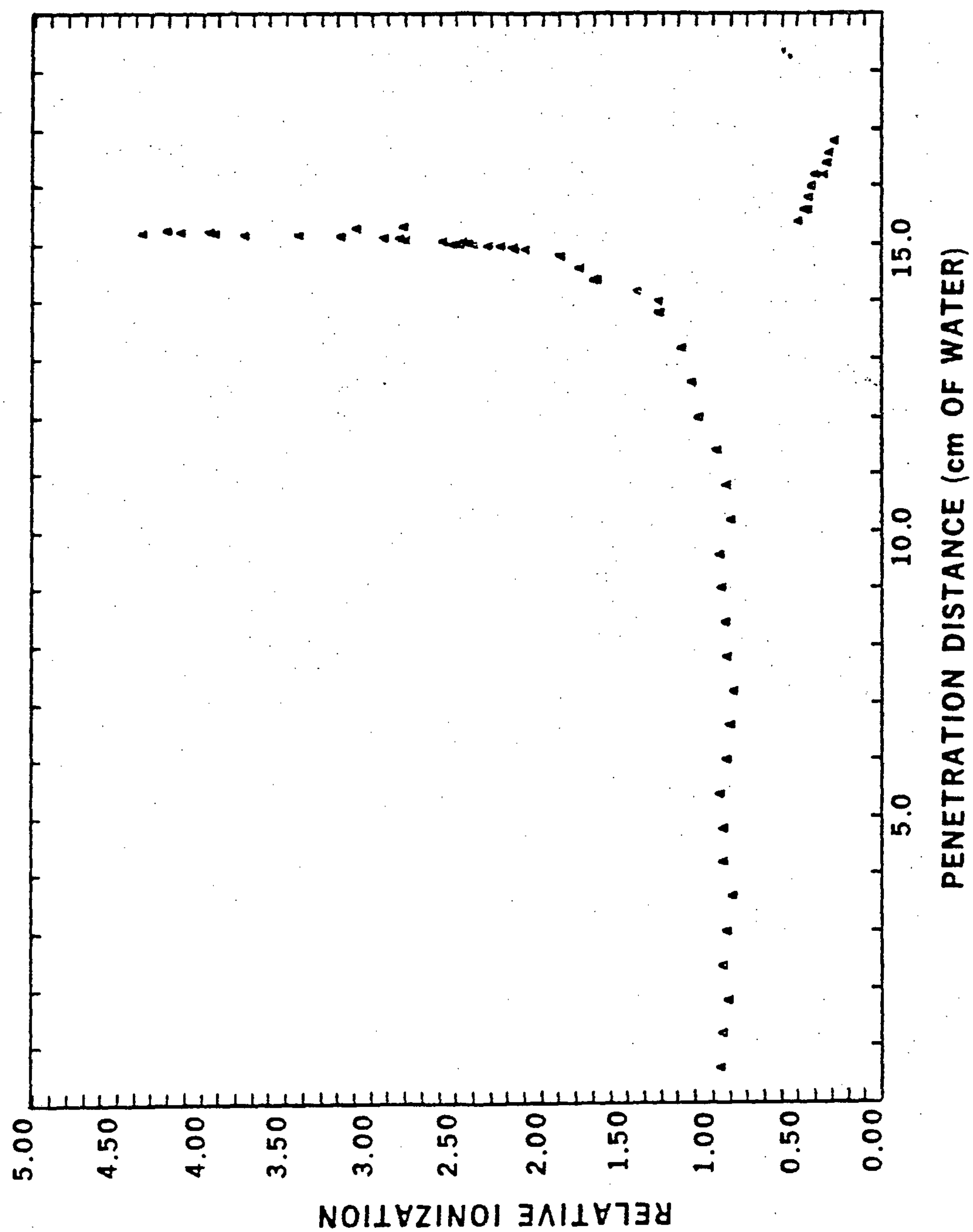
RELATIVE IONIZATION
0.00
0.50
1.00
1.50
2.00
2.50
3.00
3.50
4.00
4.50
5.00
PENETRATION DISTANCE (cm OF WATER)
5.0
10.0
15.0

XBL 819-7003

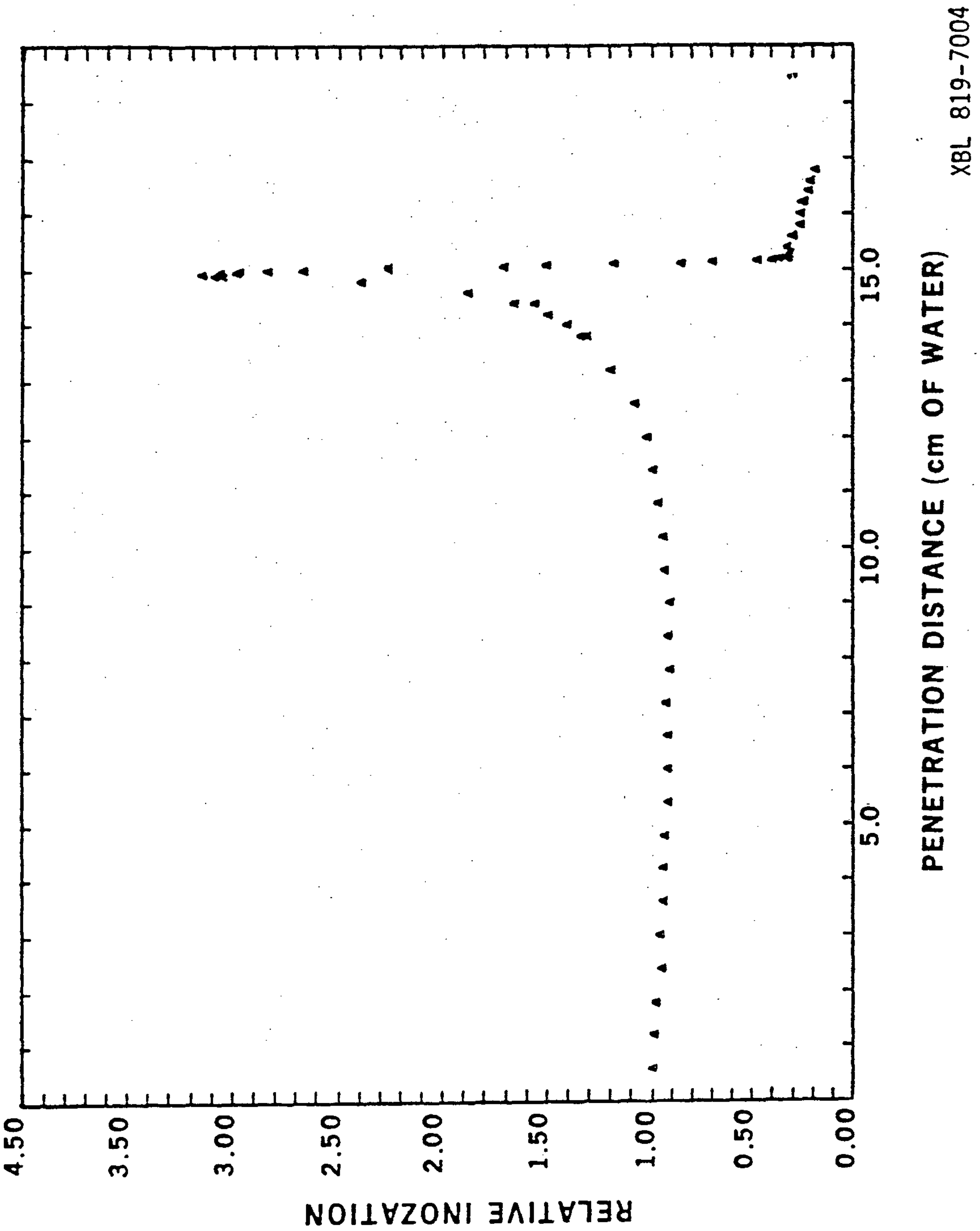
RELATIVE INOZATION
0.00
0.50
1.00
1.50
2.00
2.50
3.00
3.50
4.50
PENETRATION DISTANCE (cm OF WATER)
5.0
10.0
15.0
XBL 819-7004

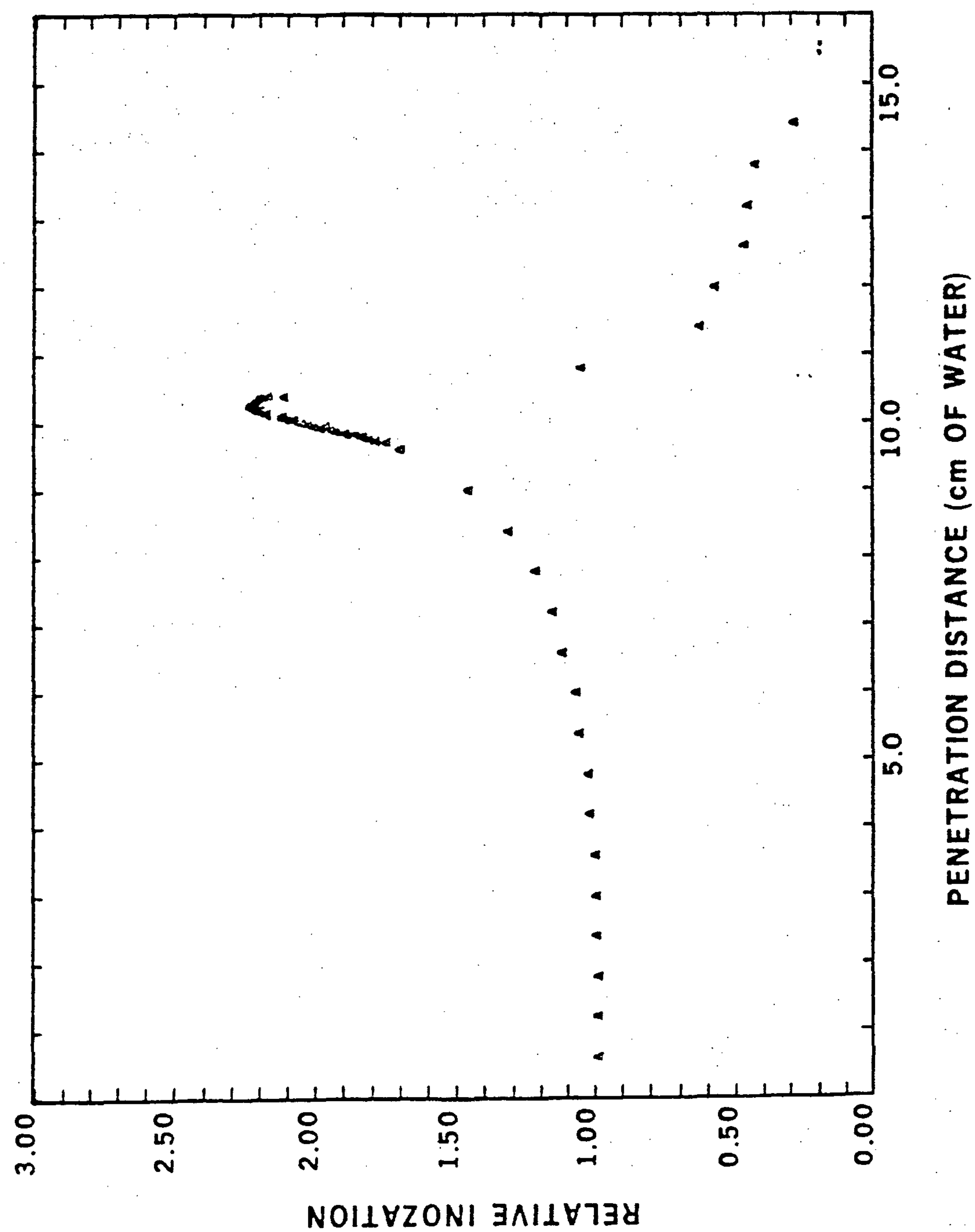
RELATIVE INOZATION
3.00
2.50
2.00
1.50
1.00
0.50
0.00
PENETRATION DISTANCE (cm OF WATER)
5.0
10.0
15.0

XBL 819-7005

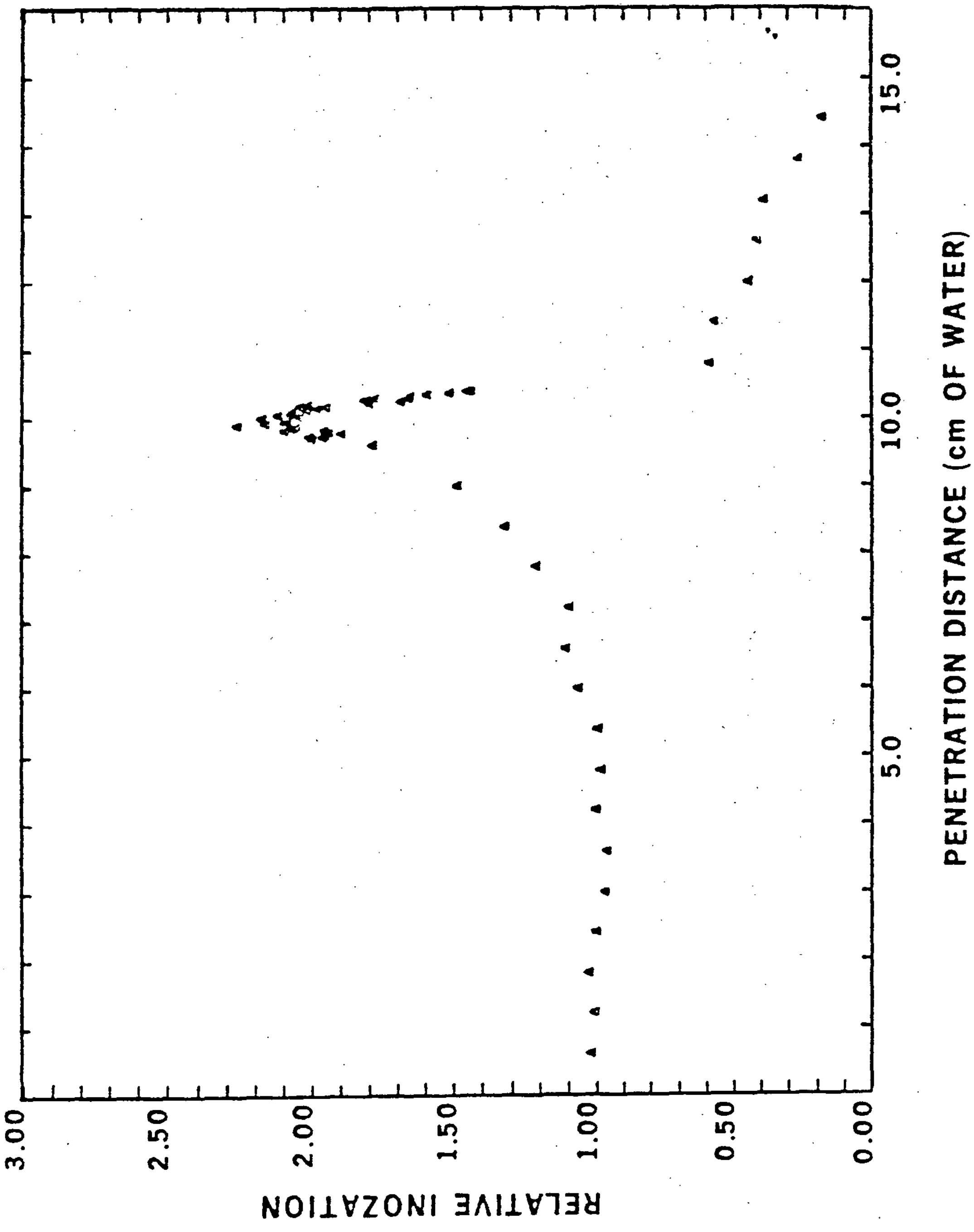
RELATIVE INOZATION
3.00
2.50
2.00
1.50
1.00
0.50
0.00
PENETRATION DISTANCE (cm OF WATER)
5.0
10.0
15.0

XBL 819-7006

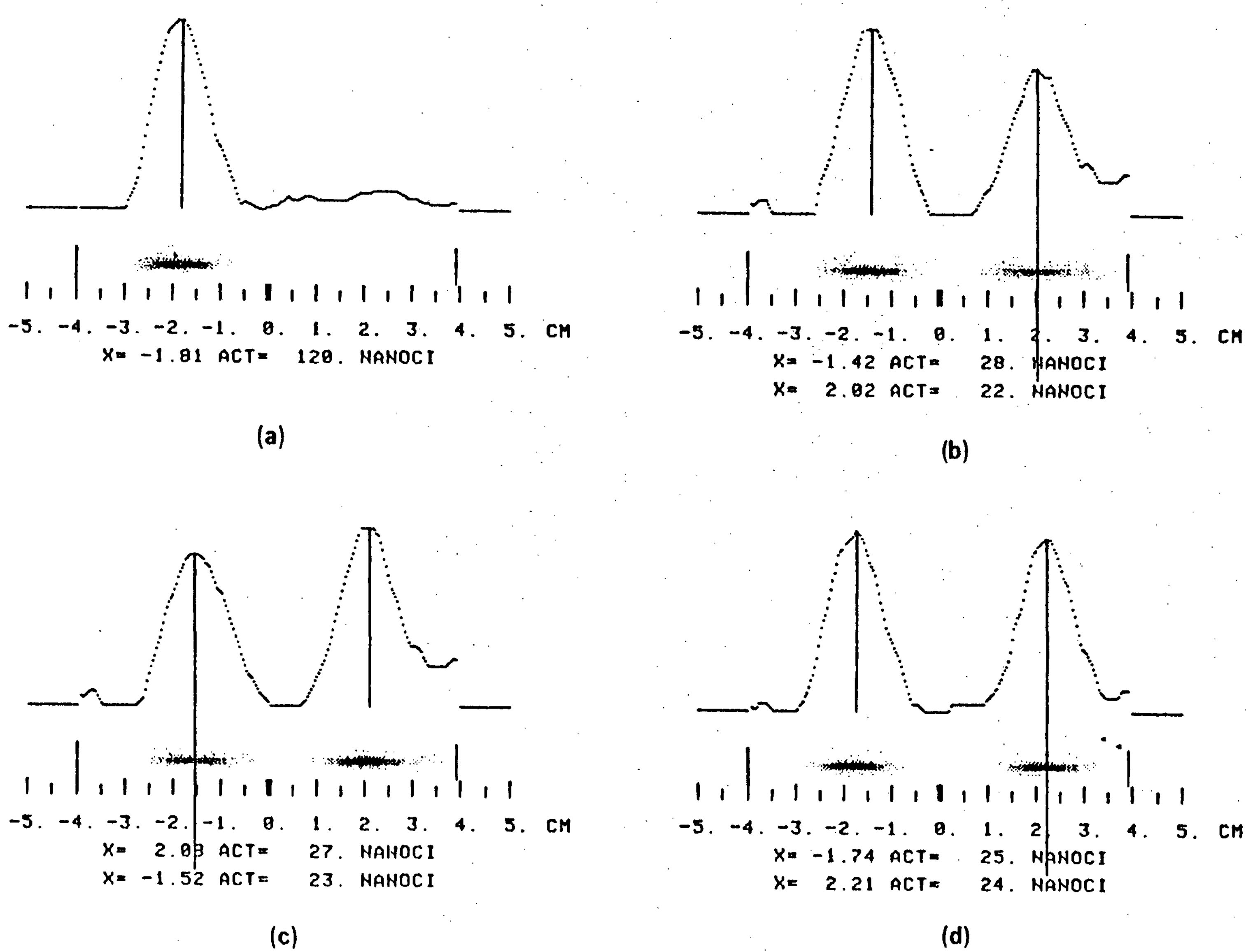

-5. -4. -3. -2. -1. 0. 1. 2. 3. 4. 5. CM
X= -1.81 ACT= 120. NANOCI
(a)
-5. -4. -3. -2. -1. 0. 1. 2. 3. 4. 5. CM
X= -1.42 ACT= 28. NANOCI
X= 2.02 ACT= 22. NANOCI
(b)
-5. -4. -3. -2. -1. 0. 1. 2. 3. 4. 5. CM
X= 2.08 ACT= 27. NANOCI
X= -1.52 ACT= 23. NANOCI
(c)
-5. -4. -3. -2. -1. 0. 1. 2. 3. 4. 5. CM
X= -1.74 ACT= 25. NANOCI
X= 2.21 ACT= 24. NANOCI
(d)

XBL 819-7001

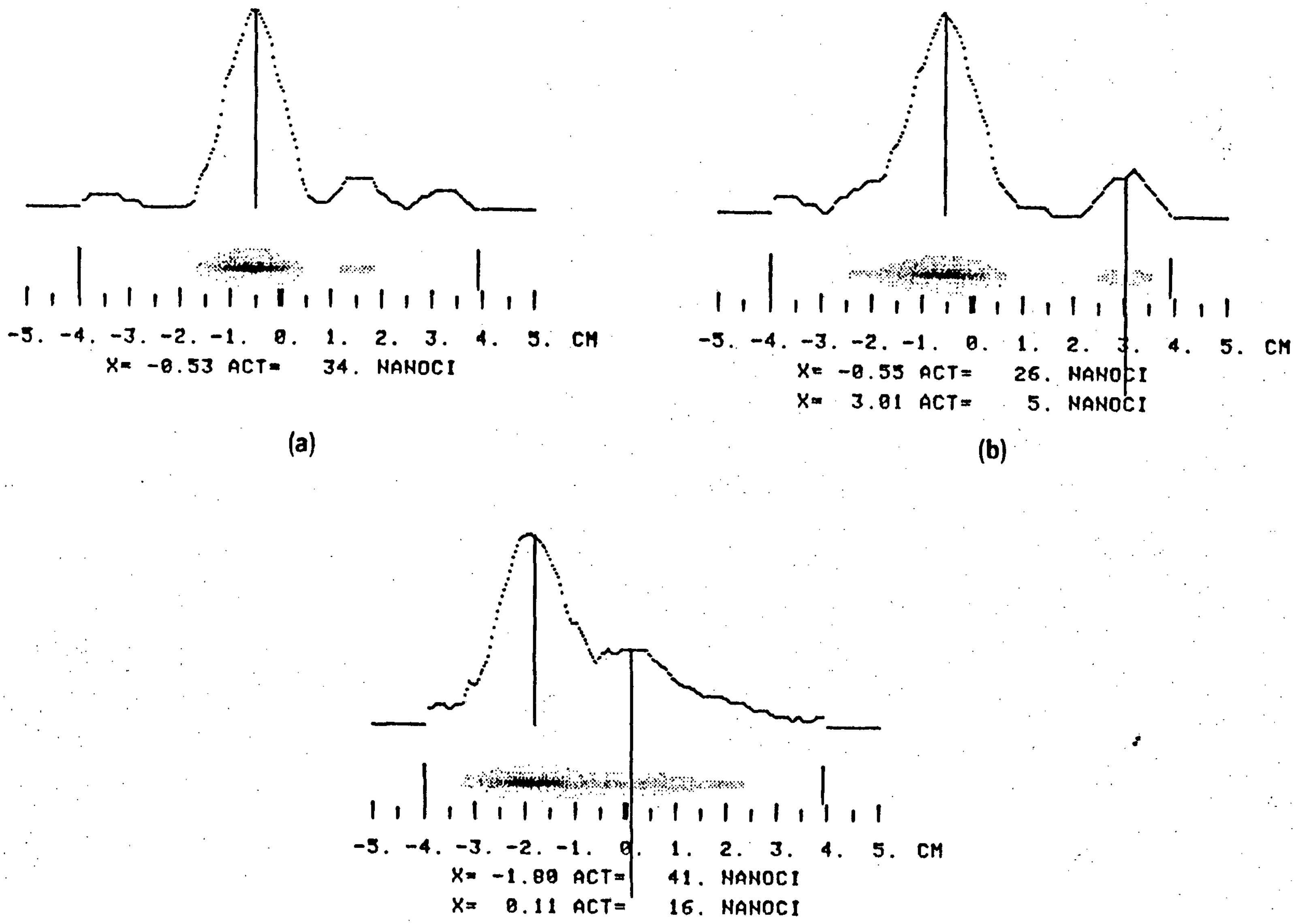

(a) (b) (c)

XBL 819-7002

TECHNICAL INFORMATION DEPARTMENT
LAWRENCE BERKELEY LABORATORY
UNIVERSITY OF CALIFORNIA
BERKELEY, CALIFORNIA 94720